https://doi.org/10.26599/FRICT.2026.9441312

Research Article

Tribological performance of catalytic ceramic conversion treated Ti-15-3 β-Ti alloy under multi-lubrication conditions

Tong Pan[a], Diandian Wu[a], Ke Ren[c*], Xiaoying Li[a], Kan Ma[b,a*], Hanshan Dong[a]

[a] School of Metallurgy and Materials, University of Birmingham, Edgbaston, Birmingham, B15 2TT, UK

[b] Department of Mechanical Engineering, City University of Hong Kong, Hong Kong, China

[c] School of Chemical Engineering, University of Birmingham, Edgbaston, Birmingham, B15 2TT, UK

[*] Corresponding authors:

Ke Ren, E-mail: k.ren@bham.ac.uk;

Kan Ma, E-mail: kan.ma@cityu.edu.hk

Received: May 5, 2026; Revised: July 27, 2026; Accepted: September 2, 2026

Abstract

The tribological behaviour of Ti-15-3 β-titanium alloy treated by integrating bulk treatment with surface functionalisation (IBTSF) was systematically investigated under unlubricated, oil-lubricated, deionised water and simulated seawater conditions. Reciprocating sliding tests were performed against a WC ball under loads of 10 N or 20 N for 10,000 cycles. The results demonstrate that the tribological performance strongly depends on both the IBTSF treatments and the test environments. Under unlubricated conditions, the catalytic ceramic conversion treatments (C3TAu32 and C3TAg32) exhibited significantly lower friction and wear than the conventional ceramic conversion treatment (C2T32), owing to the self-lubricating effect of Au/Ag and the formation of thicker oxide layers. Hence, under the most severe unlubricated sliding condition (20 N), C3TAu32 reduced the wear factor by 99% compared with C2T32. In contrast, C2T32 showed superior wear resistance in oil, deionised water and simulated seawater because of its dense oxide layer and strong oxide/substrate bonding, while C3TAg32 suffered from corrosive wear in simulated seawater. Thus, C2T32 exhibited a wear factor 90% lower than C3TAg32 under simulated seawater. These findings establish application-oriented guidelines for selecting IBTSF treatments under different service environments, with C3TAu32 recommended for unlubricated applications and C2T32 for oil-lubricated and marine environments. The possible wear mechanisms are discussed to advance scientific understanding.

Keywords: metastable β-titanium alloy; integrating bulk treatment with surface functionalisation (IBTSF); tribological behaviour; lubrication.

1. Introduction

Ti-15V-3Cr-3Al-3Sn (Ti-15-3) is a metastable β-titanium alloy that has attracted considerable interest owing to its high specific strength, excellent corrosion resistance, and good formability, making it suitable for aerospace, marine, and other high-performance engineering applications [1-4]. In many of these service environments, components are inevitably subjected to sliding or rolling contact, where resistance to friction and wear becomes a critical factor governing reliability and service life [5-8]. Despite its favourable mechanical and chemical properties, Ti-15-3 generally exhibits poor tribological performance, particularly under sliding conditions [9, 10]. The inherently low hardness and strong adhesive tendency of titanium alloys often lead to severe material transfer, high coefficient of friction, and accelerated wear [11-13]. These limitations have significantly restricted the wider use of Ti-15-3 in tribologically demanding applications, even when lubrication is applied.

To address this challenge, an environmentally friendly ceramic conversion treatment (C2T) was purposely developed by Dong et al. [14, 15]. However, C2T is not applicable for metastable β-titanium alloys due to the over-aging caused by the high temperature (600 °C) and long treatment time (80-100 h). To this end, a combined bulk and surface treatment was developed and applied to a low-cost β-titanium alloy with limited success [16]. Recently, with the development of advanced catalytic ceramic conversion treatment (C3T) which can effectively reduce the treatment temperature and time [6], a novel surface engineering strategy that integrates bulk treatment with surface functionalisation (IBTSF) has recently been proposed [10]. This concept primarily aims to achieve a synergistic improvement in surface tribological behaviour while enhancing the bulk mechanical properties of the alloy and imparting additional surface functionalities. Initial work studied the feasibility of the IBTSF technique for Ti-15-3 alloy, showing significant improvements in wear resistance under unlubricated sliding conditions for up to 1000 cycles, with

enhanced antibacterial performance. However, these exploratory investigations were primarily intended to verify the feasibility of the novel surface engineering concept rather than to establish its tribological performance under practical service conditions.

In engineering applications, titanium alloy components are commonly exposed to a wide range of operating environments, including dry sliding, oil lubrication, aqueous media and marine conditions [11, 17-20]. These environments profoundly influence interfacial lubrication, tribo-chemical reactions, wear evolution and surface degradation, meaning that tribological behaviour cannot be reliably assessed using a single testing condition. Moreover, the relatively short sliding duration adopted in previous studies is insufficient to evaluate the long-term stability and durability of the ceramic conversion layers. Consequently, a systematic understanding of the lubrication-dependent tribological behaviour and wear mechanisms of IBTSF-treated β-titanium alloys under representative service environments remains lacking.

In this work, the tribological behaviour of IBTSF-treated Ti-15-3 alloy is systematically investigated under four representative environments, namely dry sliding, oil lubrication, deionised water and simulated seawater. Wear tests were performed for 10,000 cycles to evaluate the long-term friction and wear performance. Beyond assessing tribological performance under different service conditions, this work aims to establish application-oriented guidelines for selecting appropriate catalytic ceramic conversion treatments for different lubrication environments. More importantly, the study elucidates the lubrication-dependent tribological mechanisms governing the performance of IBTSF-treated β-titanium alloy surfaces, thereby advancing the scientific understanding of environment-controlled friction and wear processes while extending the applicability of the IBTSF technique towards practical engineering applications.

2. Experimental

2.1 Material and sample preparation

The β-titanium alloy rods of Ti-15V-3Al-3Cr-3Sn (Ti-15-3, National Institute of Standards and Technology, United States), which has the following composition (wt.%): 15% V, 3% Al, 3% Cr, 3% Sn, and balance Ti, were abrasion cut (Struers Accutom 50) using cubic boron nitride cutting wheels to produce 5 mm thick cylindrical samples. Samples were subsequently flattened and ground (up to #1200 grit size) using SiC abrasive paper. Ultrasonic cleaning using liquid detergent and acetone were carried out to remove contaminants between each stage.

2.2 Combined C3T and bulk aging treatment

In our previous work [10], a novel surface engineering strategy that integrates bulk treatment with surface functionalisation (IBTSF) has been successfully developed for the β-titanium alloy of Ti-15-3. The process begins with a pre-solution treatment at 850 °C for 1 h to achieve a fully β-phase microstructure. Then, the porous surface oxide layer with low bonding to the substrate formed during high-temperature solution treatment was removed, followed by deposition of a ~20 nm Au or Ag catalytic layer. Finally, a combined surface C3T-substrate aging treatment was applied at 538 °C for 32 h to generate multilayered surface systems (i.e. C3TAg32 and C3TAu32), enabling simultaneous enhancement of surface performance and bulk mechanical properties. The surface layer structures and the related characteristic features are summarised in **Figure 1** to provide essential information for the understand of their tribological behaviours under different environmental conditions. For comparison, conventional ceramic conversion treatment (C2T) without pre-deposition of any catalytic layers was also carried out at the same temperature of 538 °C and for the same time of 32 h for C2T32 sample.

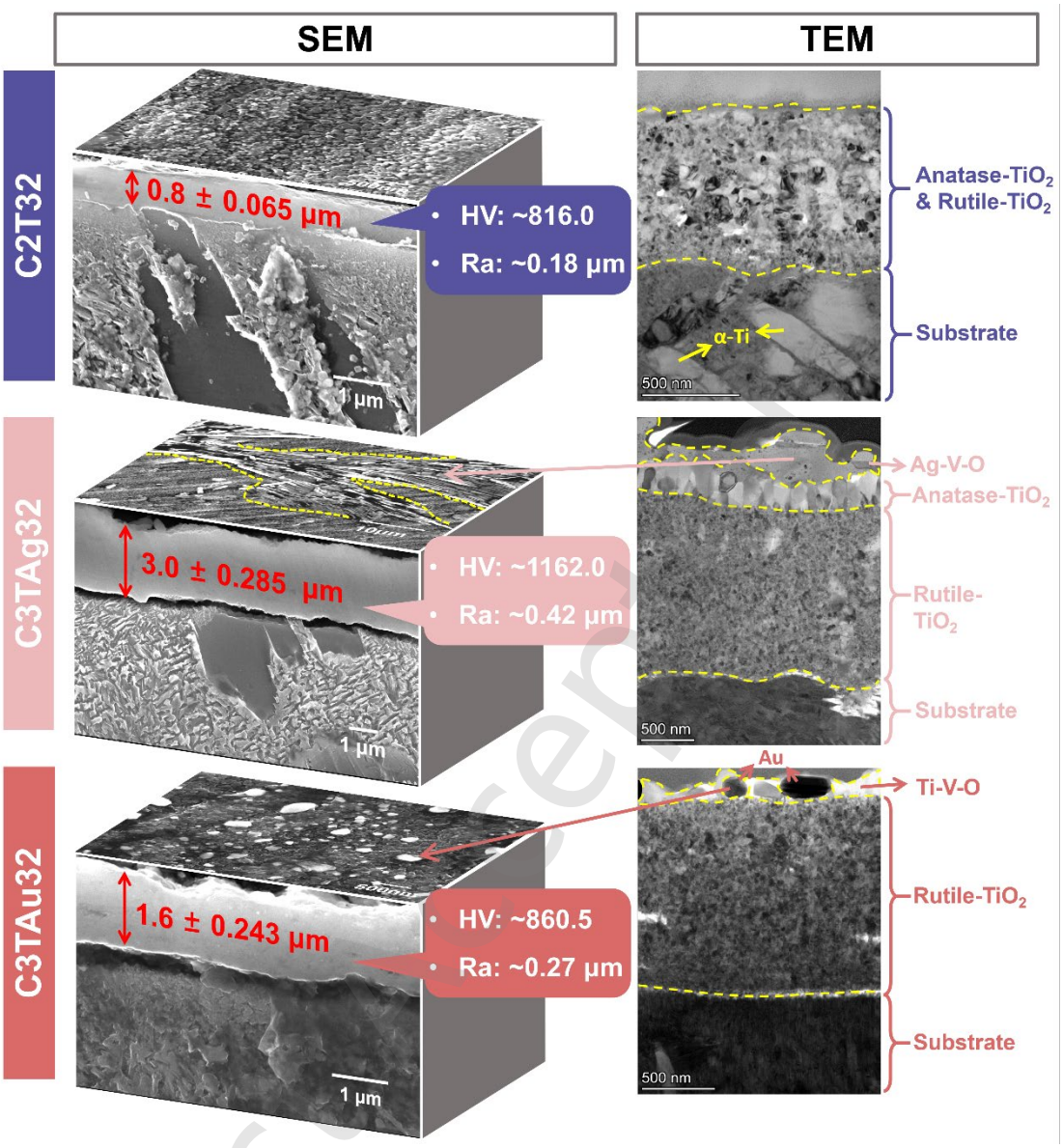

Figure 1. Cross-sectional SEM and TEM microstructures of three IBTSF-treated Ti-15-3 surface systems (C2T32, C3TAg32 and C3TAu32), showing characteristics of the three different surface layer structures. Information of the layer hardness, thickness and roughness are indicated. Detailed information can be found in our early publication paper of reference [10].

SEM images revealed a dense featureless surface layer with 0.8, 3.0 and 1.6 µm thickness for C2T32, C3TAg32 and C3TAu32 samples respectively. It is clear that Au and Ag additive catalytic layer increased the surface layer thickness by 2.0 and 3.8 times to that of the C2T32 sample under the same treatment temperature and duration.

TEM with SAD patterns analysis unveiled the detailed phase compositions and layer structures of these investigated three samples. For C2T32 sample, a multi-grain layer with a mixture of anatase-TiO_2 and rutile-TiO_2 formed on the top of oxygen diffusion layer, where some slabs of α-Ti transformed from β-Ti. Interestingly, additive layer of Ag and Au boosted the rutile-TiO_2 layer growth without stimulating the grains size (between 20 ~ 80 nm). At the meantime, a different distinct top layer form on TiO_2 layer of C3TAu32 and C3TAg32 samples. As denoted in **Figure 1**, Ag introduced Ag-V-O oxide layer and underneath columnar anatase-TiO_2 layer. While Au particles embedded in Ti-V-O oxides formed a composite top layer. An oxygen diffusion layer beneath the top oxide layer was formed for all three samples but with the thickness of 10 ~ 20 μm for C2T32, 3 ~ 5 μm for C3TAg32 and 0 ~ 1 μm for C3TAu32 samples, respectively.

2.3 Tribological performance evaluation

To investigate the frictional behaviour and wear resistance of the three samples (C2T32, C3TAg32, and C3TAu32), reciprocating sliding tests were conducted in different lubrication environments: unlubricated, oil (Shell Rimula R4 X diesel engine oil, 15W-40), simulated seawater (3.5 wt% NaCl solution, hereafter SSW), and de-ionised water (hereafter DI water). All the tests were performed at room temperature (22~26 °C) with a relative humidity of 50~55% using a TE-79 multi-axis tribology machine (Phoenix Tribology, UK). An 8 mm diameter Grade 5 tungsten carbide (WC) ball (diameter tolerance: ± 0.2 μm) was used as the counterpart. Reciprocating sliding tests were conducted under normal loads of 10 or 20 N for 10,000 cycles at a sliding speed of 5 mm/s and an amplitude of 5 mm. For lubricated tests, a sufficient volume of lubricant was used in order to completely immerse the specimen throughout the experiment. For each test condition, three repeated tests were conducted to ensure statistical reliability. Prior to testing, the tribometer was calibrated following the procedure from the manufacturer to ensure the accuracy of the applied normal

load and friction force measurements.

The 3D wear morphology was characterised using the white light interferometer (Profilm3D, KLA Corporation, California, USA) equipped with a Nikon CF Plan objective lens (Nikon Corporation, Japan). The wear factor (K, $m^3/N \cdot m$) was calculated by the formula:

$$K = \frac{V}{F \times s} = \frac{A \times 5 \times 10^{-3}}{F \times s} \quad (1)$$

where V is the wear volume (m^3), F is the applied load (N), s is the sliding distance (m), A is the cross-sectional area of the wear scare (m^2).

All quantitative data are presented as the mean ± standard deviation (SD) based on three independent measurements (n = 3), unless otherwise stated. Comparisons between two groups, e.g., **Figure 5** and **Figure 6c**, were performed using an unpaired two-tailed t-test. Comparisons among three or more groups were conducted using one-way analysis of variance (ANOVA) (**Figure 2e**, **Figure 3b**, **Figure 7c**, and **Figure 8c**). Differences were considered statistically significant when $P < 0.05$. Statistical analyses were performed using GraphPad Prism 10.0 (GraphPad Software, San Diego, CA, USA).

2.4 Microstructure characterisation

Scanning electron microscopy (SEM) combined with energy-dispersive X-ray spectroscopy (EDX) was employed to examine the wear morphology and elemental distribution on both the wear tracks and the corresponding WC counter-face. Analyses were performed using a Thermo Fisher Scientific Apreo 2S HiVac field-emission SEM (Thermo Fisher Scientific, USA).

Cross-sectional TEM lamellae were prepared using a focused ion beam-scanning electron microscope (FIB-SEM, DB550, CIQTEK, China) by the in-situ lift-out method. The microstructure and phase constitution of the surface oxide layers were subsequently characterised using a Talos F200X G2

transmission electron microscope (TEM, Thermo Fisher Scientific, USA) operated at an accelerating voltage of 200 kV.

2.5 Electrochemical and scratch tests

The corrosion behaviour of the C3T treated Ti-15-3 surfaces was investigated using a Gamry electrochemical workstation equipped with a saturated calomel reference electrode (SCE, Hg/Hg_2Cl_2) and a platinum counter electrode. All electrochemical tests were conducted in naturally aerated SSW at room temperature. Prior to polarisation testing, each sample (exposed surface area ~0.504 cm^2) was immersed in the electrolyte for 3600 s to stabilise the open-circuit potential (OCP).

Potentiodynamic polarisation curves were subsequently recorded in the potential range from −0.5 V to +1.5 V versus SCE at a scan rate of 1.67 $mV \cdot s^{-1}$. Corrosion potential (Ecorr) and corrosion current density (Icorr) were obtained through Tafel extrapolation.

Scratch tests were performed using a Scratch Tester (CSM A02-143b, CSM Instruments, Switzerland) equipped with a Rockwell diamond indenter (radius: 200 μm) to evaluate the mechanical integrity of the surface oxide layers and the bonding between the surface oxide layer and the subsurface. Progressive-load scratches were carried out with the normal load increasing linearly from 0 to 20 N at a loading rate of 100 N/min over a scratch length of 2 mm and a scratching speed of 10 mm/min. During the tests, both acoustic emission (AE) and tangential force were continuously recorded to monitor the onset of fracture and interfacial failure of the surface layers.

3. Results

3.1 Tribological behaviour under unlubricated condition

3.1.1 Friction and wear

Figure 2 presents the unlubricated sliding wear results of the three samples (C3TAu32, C3TAg32, and C2T32) tested under 10 N and 20 N loads for 10,000 cycles, including their coefficient of friction (COF), 3D wear track topographies, cross-sectional wear track profiles, and wear factor comparisons.

As shown in **Figure 2a**, under a load of 10 N, the COF of C2T32 increases sharply to ~0.4 within the first 1000 cycles, followed by a slower rise, eventually stabilising around 0.55 after 4000 cycles. In contrast, both C3T samples exhibited significantly lower COF: the COF of C3TAg32 remained steady at ~0.25 in 1000~1500 cycles, then gradually increased to ~0.4 before 5000 cycles, and finally reached ~0.45 at 10,000 cycles; the C3TAu32 maintained a low COF of ~0.25 until 4000 cycles, and increased slightly to ~0.38 until 10,000 cycles.

To further explore the wear resistance, the applied load was doubled to 20 N while maintaining identical the rest of test conditions. **Figure 2b** shows that both C2T32 and C3TAg32 exhibit highly fluctuating COF distributions, starting around 1000 and 3000 cycles respectively, and continuously increasing up to ~0.65 ± 0.15 after 10,000 cycles. This high and fluctuating COF is typical for untreated Ti and its alloys, which implies the breakdown of the surface protective oxide layer, thus exposing the titanium substrate and leading to unstable adhesive wear. In contrast, C3TAu32 maintained a highly stable COF throughout the entire test with only a very small increase (~0.02) compared to the results under 10 N condition, even after 10,000 cycles.

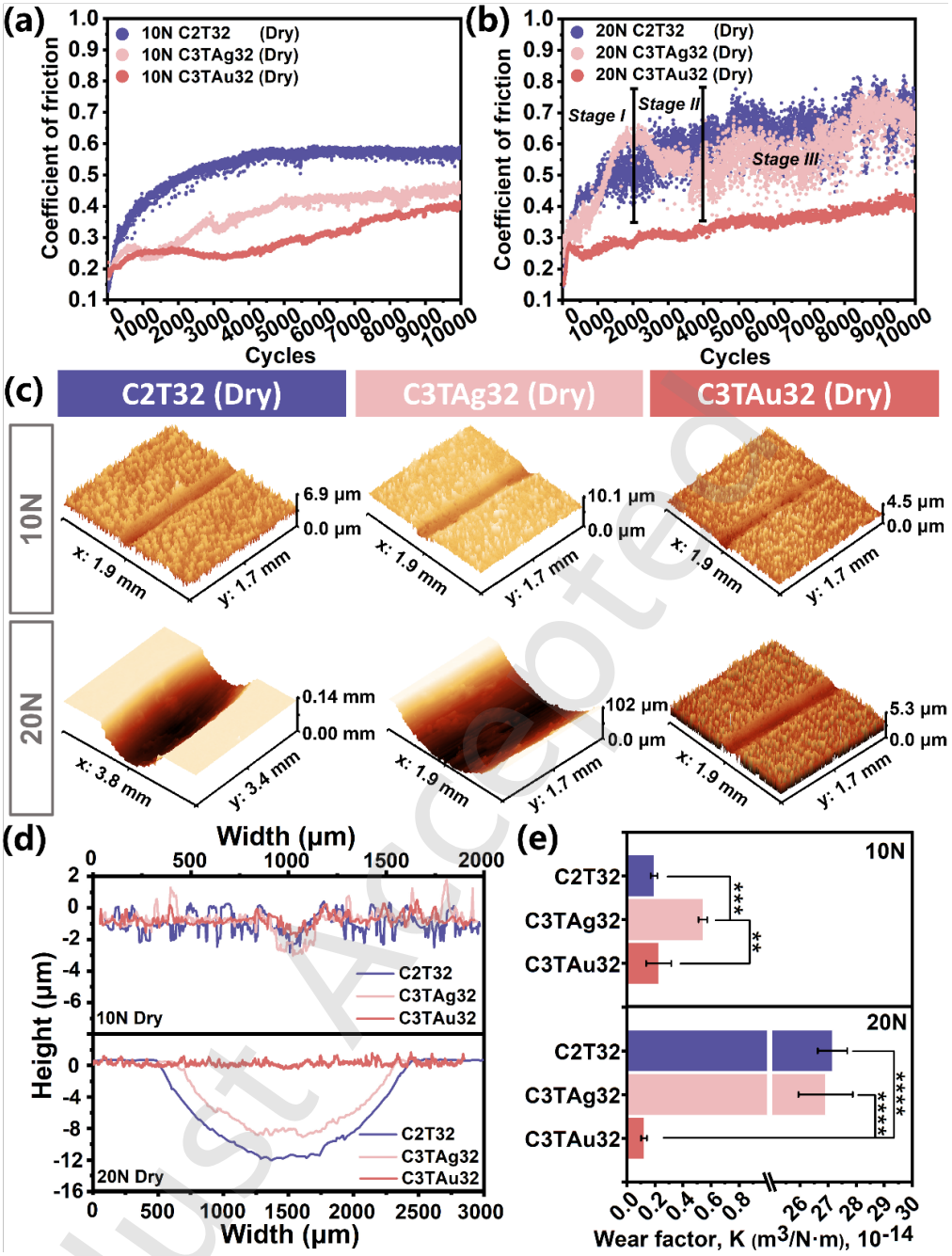

Figure 2. Tribological performance of the three IBTSF-treated Ti-15-3 surface systems under unlubricated conditions: (a) COF under a load of 10 N; (b) COF under a load of 20 N; (c) 3D wear track morphologies after the 10 N and 20 N wear tests; (d) corresponding 2D wear track profiles used for wear volume determination; (e) wear factors calculated from the wear track profiles. Error bars represent the standard deviation of three independent measurements (mean ± SD, n = 3). Statistical significance was analysed using one-way ANOVA (**$p<0.01$, ***$p<0.001$, and ****$p<0.0001$).

Figure 2c and **Figure 2d** compare the wear track 3D topographies and corresponding cross-sectional profiles of the three samples after 10,000 cycles under 10/20 N loads. When tested under 10 N, all three samples showed very shallow wear depths, with C3TAg32 exhibiting the deepest wear depth (~2 μm), followed by C2T32 (~1.5 μm) and C3TAu32 (~1 μm). This demonstrates that the oxide layers formed by both C2T and C3T can protect Ti-15-3 from severe wear. However, when tested under 20 N, the differences become more pronounced: C3TAg32 and C2T32 display substantially larger wear areas with the depths of ~8 μm and ~12 μm, respectively, whereas the wear track depth of C3TAu32 remained unchanged, with a depth of ~1 μm. Accordingly, it is clear that C3TAu32 exhibited superior friction stability and wear resistance. The quantified wear factors (**Figure 2e**) further confirm this behaviour: C3TAu32 showed an extremely low wear factor of approximately 0.2×10^{-14} $m^3/(N \cdot m)$ under 10 N, which is decreased to half due to the nearly constant wear volume and the increased load of 20N. In contrast, the wear factors of C2T32 and C3TAg32 under 20 N are more than 250 times higher than that of C3TAu32, and even under 10 N, C3TAg32 showed a wear factor more than twice that of C3TAu32.

As shown in **Figure 2b**, the C3TAg32 sample exhibits a pronounced variation in the coefficient of friction (COF) under 20 N. To investigate the underlying mechanisms, wear tests were conducted at 3 representative stages corresponding to distinct COF behaviours: 1000 cycles (Stage I – rising), 3000 cycles (Stage II – decreasing), and 10, 000 cycles (Stage III – fluctuating). The corresponding results are presented in **Figure 3**.

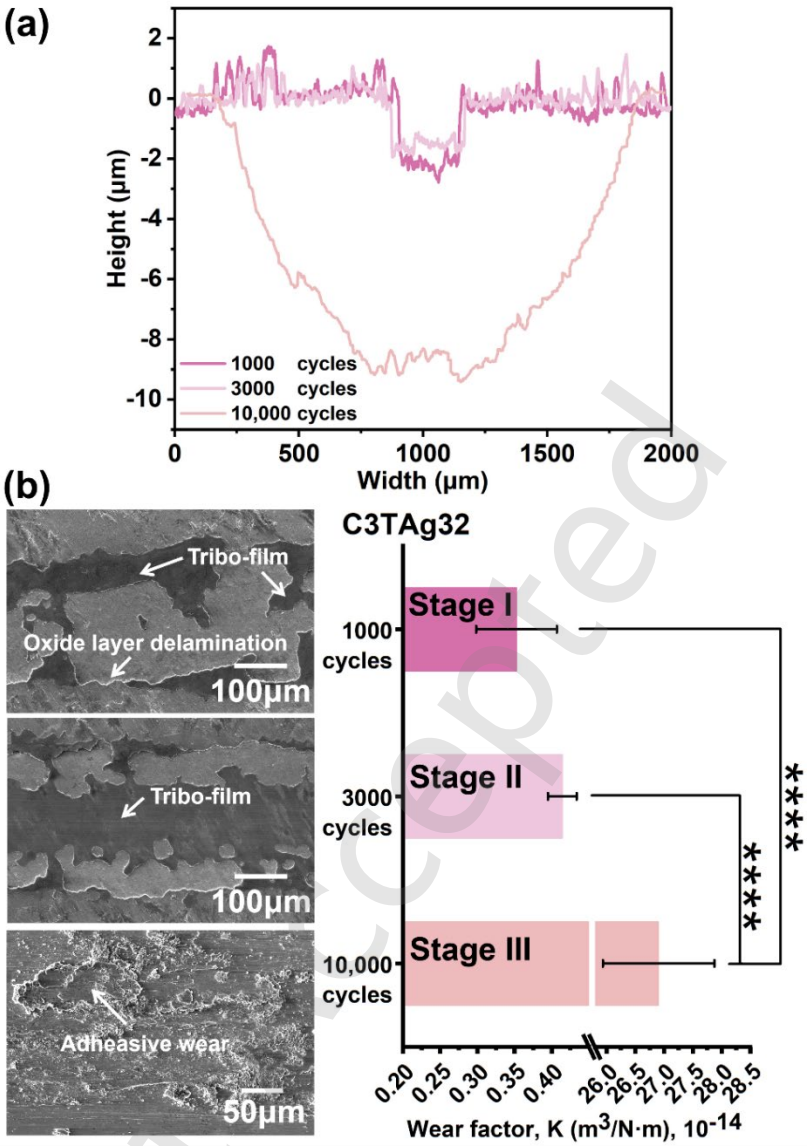

Figure 3. Evolution of the tribological behaviour of C3TAg32 during unlubricated sliding, showing the three characteristic wear stages: (a) 2D wear track profiles corresponding to Stages I – III; (b) SEM images of the wear tracks at different wear stages and the corresponding wear factors. Error bars represent the standard deviation of three independent measurements (mean ± SD, n = 3). Statistical significance was analysed using one-way ANOVA (****p < 0.0001).

The results show that during Stage I and Stage II (**Figure 3a**), the surface oxide layer remained largely intact, with only the asperity peaks being gradually removed by the WC ball, resulting in progressive widening of the wear track.

The oxide wear debris generated during this process accumulated within the contact region and initiated the formation of a tribo-film. SEM images reveal that in Stage I, the tribo-film was only locally formed and discontinuously distributed over the wear track, producing a pronounced surface height difference between the film-covered and directly contacted regions. Consequently, the real contact conditions remained unstable, leading to a continuous increase in the COF.

As sliding proceeded, more wear debris was compacted into the contact surface, and during Stage II a continuous, dense and smooth tribo-film gradually developed, covering the main contact area between the WC ball and the wear track. The formation of this compact tribo-film effectively separated the counterpart from the oxide surface, reducing direct asperity contact and resulting in a gradual decrease in the COF.

However, under prolonged reciprocating sliding, the newly formed tribo-film and/or the underlying titanium alloy became susceptible to local fatigue failure. Once the compact, smooth and continuous tribo-film was locally disrupted, large amounts of compacted hard wear debris were generated. These debris particles acted as third-party abrasives, promoting severe abrasive wear and accelerating the degradation of the surface oxide layer. Consequently, the titanium substrate became exposed, leading to severe adhesive wear accompanied by a gradual increase in the COF during Stage III.

The wear factor data across these 3 stages reveal a steady increase with the wear stage, rising from 0.35×10^{-14} m³/(N·m) in Stage I through 0.42×10^{-14} m³/(N·m) in Stage II to 2.68×10^{-13} m³/(N·m) in Stage III, consistent with the progressive failure of the protective oxide and tribo-film layers.

3.1.2 Wear morphologies

To further investigate the friction and wear behaviour and the underlying wear mechanisms, **Figure 4** presents the wear track morphologies of these 3

samples after wear tests under 10 N or 20 N, with the corresponding wear scars on the WC balls after sliding against the treated surface under 20 N. As shown in **Figure 2c**, all three samples endured 10,000 cycles of unlubricated wear under 10 N. The wear scars on the WC balls after sliding against three different samples exhibited similar morphologies, containing only mild, directional scratches without obvious material transfer. This indicates that all 3 samples successfully transformed the typical adhesive wear behaviour of Ti-15-3 titanium alloy into mild abrasive wear.

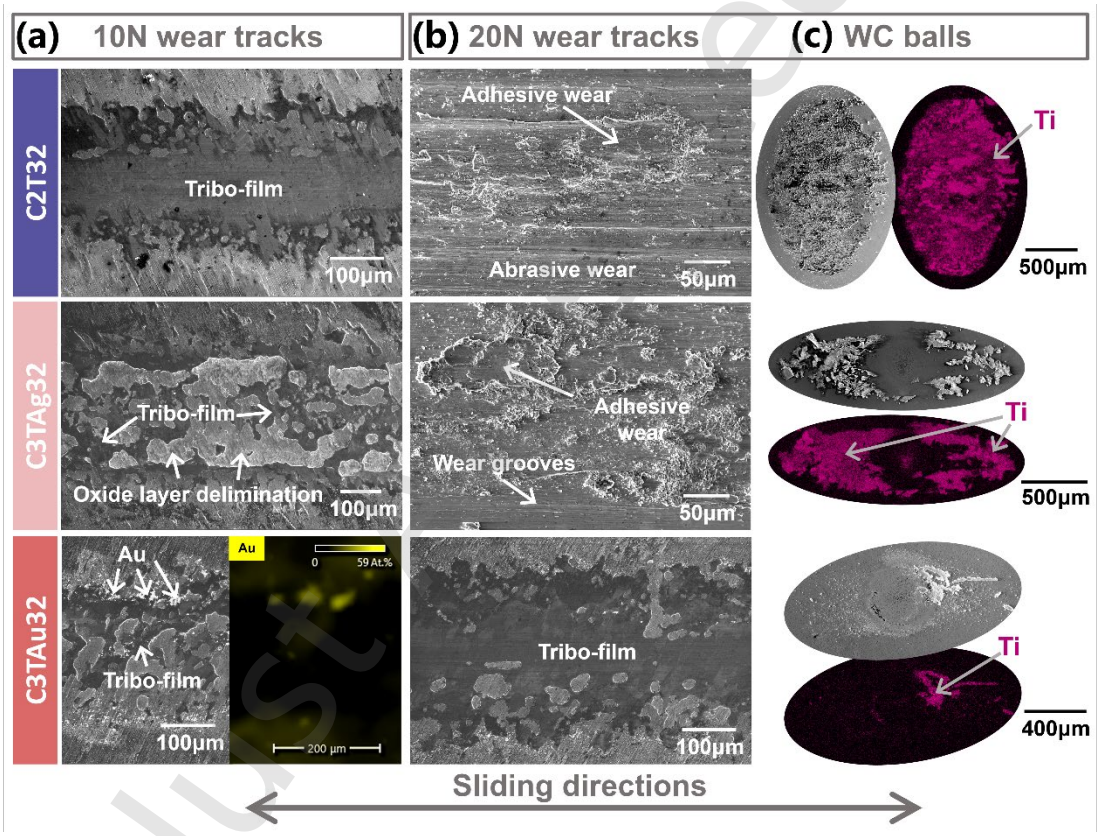

Figure 4. SEM images of the wear tracks and counterpart wear scars after unlubricated sliding tests: (a) SEM images of C2T32, C3TAg32 and C3TAu32 after testing under a load of 10 N, with Au element (EDX) mapping; (b) SEM images after testing under a load of 20 N; (c) SEM images of the corresponding wear scars on the WC counterpart balls after the 20 N tests, with Ti elemental (EDX) mapping.

As shown in **Figure 2d** and **Figure 4a**, the oxide layers formed on these three samples still remained but suffered varying degrees of wear damage. The C2T32 sample formed and preserved a continuous tribo-film, which explains its shallow wear depth in **Figure 2d**; C3TAu32 also exhibited a shallow wear track, attributed to the solid lubrication effect of Au particles on the oxide layer surface [21], which can still maintain excellent wear resistance even partial delamination of the tribo-film occurred. In contrast, C3TAg32 showed the deepest wear depth (**Figure 2d**) probably due to severe oxide layer spallation. This is because Ag and the alloying elements in Ti-15-3 with strong affinity with oxygen (such as V and Al) are oxidised to form columnar grains in the upper region of the oxide layer during the C3T process [10]. Owing to their relatively low strength and high brittleness, these columnar grained layers are prone to fracture under sliding contact, generating hard wear debris as third-party abrasive particles to cause potential severe abrasive wear.

When the load was increased to 20 N (**Figure 4b, c**), the wear behaviour of both the samples and the WC counterparts changed notably. EDX mapping revealed that C2T32 experienced the most severe adhesive wear, with a large amount of titanium adhered to the WC wear scar. Transfer of Ti to the WC counterpart was also observed for both C3T samples but it is much less—especially for C3TAu32. The worn surfaces corroborated these findings: C2T32 and C3TAg32 showed complete removal of their surface oxide layers, as evidenced by the very large wear depth of ~9 and ~12 μm for C3TAg32 and C2T32 respectively (**Figure 2d**); large adhesion lumps and craters were observed on their wear tracks, which are typical adhesive wear features of titanium alloys. In contrast, C3TAu32 displayed a more continuous and compact tribo-film than that formed under 10 N. This can be attributed to the higher load applied, which compacted more wear debris onto the wear track surface to form the more continuous tribo-film with increased interfacial bonding

strength. Consequently, the wear track surface was better protected, maintaining a shallow wear depth of approximately 1 μm (**Figure 2d**).

3.1.3 Wear debris

Due to the severe wear exhibited by C2T32 and C3TAg32 under the 20 N load (**Figure 4b, c**), their wear debris after 10,000 cycles was collected and analysed by SEM-EDX to further explore the mechanisms involved. As shown in **Figure 5**, the wear debris of both samples is primarily composed of the Ti-15-3 substrate (such as Ti and V), mixed with small amounts of oxygen possibly due to in-situ oxidation by the high flash temperature generated during the unlubricated wear tests.

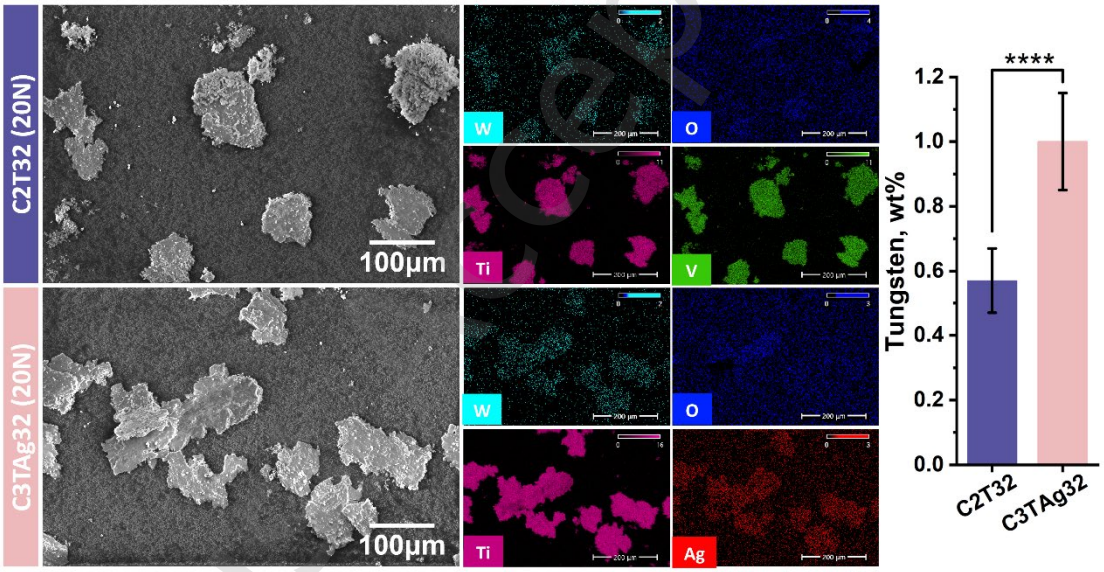

Figure 5. SEM images, EDX mapping, and quantitative elemental analysis of the wear debris collected from C2T32 and C3TAg32 after unlubricated sliding under a load of 20 N. Error bars represent the standard deviation of three independent measurements (mean ± SD, n = 3). Statistical significance was analysed using t-test (****p < 0.0001).

Interestingly, debris from both samples also contained measurable amounts of W, implying that abrasive wear may have occurred during the early wear stage, before the complete removal of the oxide layer, allowing W from the WC ball to be embedded into the debris. Quantitative EDX analysis showed that the W

content in the debris produced from C3TAg32 is nearly twice that from C2T32, indicating that the WC balls experienced more severe abrasive wear when sliding against C3TAg32 than against C2T32. This observation is in line with abrasive wear theory [22], as evidenced by the fact that C3TAg32 exhibited a significantly higher surface hardness (~1200 HV) compared with that for C2T32 (~800 HV) (see **Figure 1**) [10]. The higher hardness of C3TAg32 would promote more aggressive micro-cutting interactions at the real contact surface when sliding, thereby increasing the severity of abrasive wear.

3.2 Tribological behaviours in three types of fluids

While the above experiments were conducted under unlubricated condition have provided some useful information from fundamental research point-of-view, additional wear tests were performed in fluids including lubricating fluid of oil and non-lubricating fluids of water (SSW and DI water) to evaluate the applicability of these 3 surface systems under more realistic conditions with oil lubrication or in and non-lubricating fluids.

3.2.1 Oil lubrication

The evolution of coefficient of friction with test cycles, wear results in terms of wear track profiles and wear factors, and the wear track morphologies after wear tests under oil lubricated conditions under 20 N for 10,000 cycles are shown in **Figure 6**.

As presented in **Figure 6a**, all 3 surface systems exhibited excellent friction behaviour under oil lubrication. Their coefficients of friction remained stable at approximately 0.1 with nearly negligible fluctuations, in obvious contrast to their unlubricated frictional performance (**Figure 2a**). However, the cross-sectional wear profiles in **Figure 6b** reveal that their wear resistance differed significantly—and behaved almost opposite to the trends observed under unlubricated conditions (**Figure 2d**). C2T32 showed the best performance, with

the wear depth remaining within the range of surface roughness, indicating essentially no detectable wear. In contrast, both C3T samples displayed measurable wear depths of approximately 2 μm for C3TAg32 and 1 μm for C3TAu32.The potential mechanisms involved will be discussed in **Section 4**.

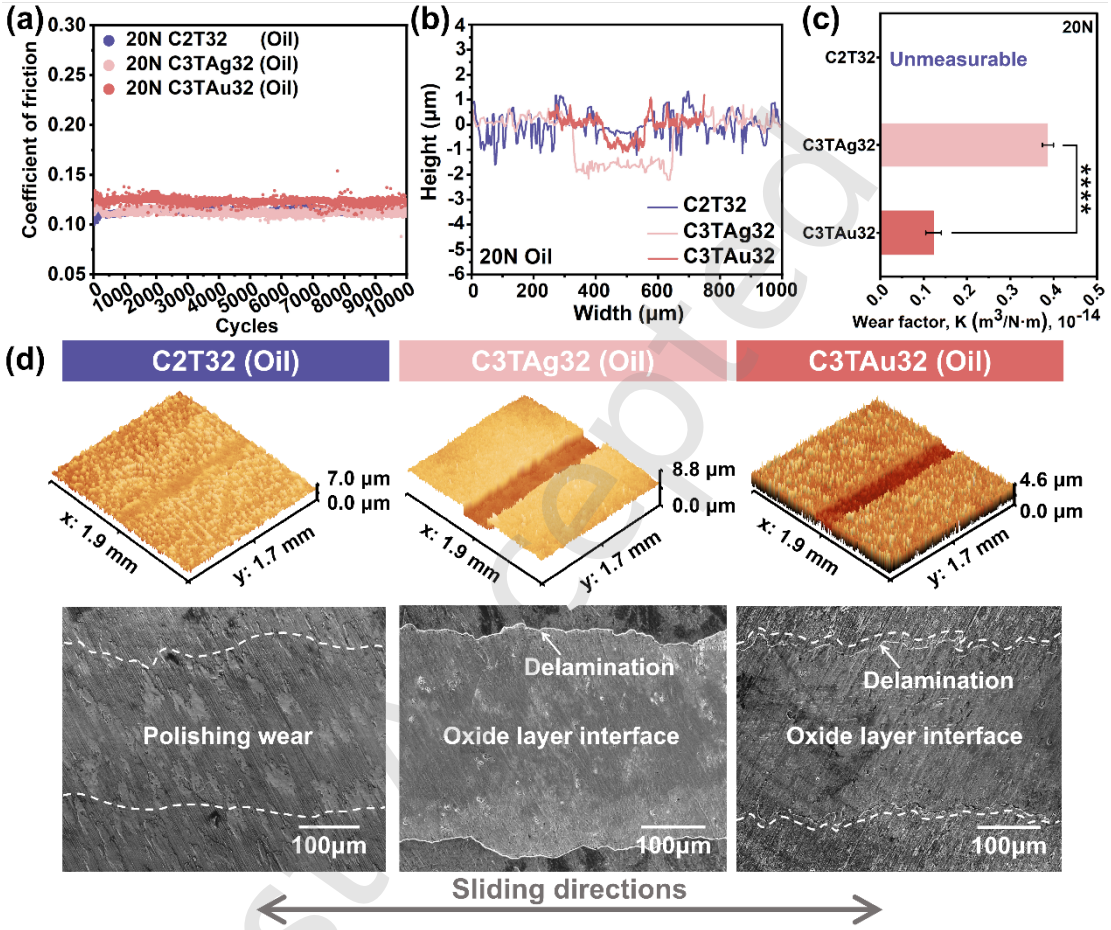

Figure 6. Tribological performance of the three IBTSF-treated Ti-15-3 surface systems under oil-lubricated conditions during sliding under a load of 20 N. (a) COF; (b) 2D wear track profiles; (c) wear factors calculated from the wear track profiles; (d) 3D wear track morphologies and the corresponding SEM observations of the wear tracks. Error bars represent the standard deviation of three independent measurements (mean ± SD, n = 3). Statistical significance was analysed using t-test (****p < 0.0001).

The wear factors were compared in **Figure 6c**. Apart from C3TAu32, whose wear factors remained similar to that obtained under unlubricated condition

(~0.1) (**Figure 2e**), the wear factors for C2T32 and C3TAg32 were significantly lower than those under unlubricated conditions: the wear factor of C2T32 was too low to be measured (vs. ~0.27 in unlubricated condition), and that of C3TAg32, although the highest among the 3 samples (~0.4), was dramatically lower than its unlubricated wear (~27). These results indicate that C2T exhibits superior wear resistance compared to both C3T treatments under oil lubrication.

Figure 6d shows the corresponding wear morphologies, which provide insight into the wear mechanisms. The counter-face WC balls exhibited almost identical features across all samples, clean surfaces without material transfer and without parallel scratches aligned with the sliding direction, confirming the absence of adhesive wear with only very mild abrasive wear.

For C2T32, the wear track showed no discernible loss of its oxide layer with some polishing effect. In contrast, both C3T samples clearly exhibited oxide layer delamination, with the thickness of the removed oxide closely matching their respective oxide-layer thicknesses. Additionally, the physical nature of the oil lubricant prevented wear debris from consolidating into a tribo-film. As a result, both C3T samples showed full exposure of the underlying substrate across the entire wear track region (**Figure 6d**).

3.2.2 In de-ionised water

To further evaluate the tribological behaviour of the 3 surface systems, reciprocating wear tests were conducted in DI water. The outcomes can also serve as the bench mark for studying the corrosion effect during the wear tests in SSW (see **Section 3.2.3**). The resulting coefficients of friction are shown in **Figure 7a**. Compared with the results under unlubricated condition, all samples exhibited significantly lower coefficients of friction owing to the lubrication effect of the DI water environment, although their COF remained higher than to that achieved under oil lubrication (**Figure 6a**). Notably, none of the samples showed the highly dispersed COF behaviour observed for unlubricated

samples under 20 N (**Figure 2b**), indicating a considerable improvement in frictional stability for both C2T32 and C3TAg32. C2T32 reached a steady COF of ~0.35 after ~2000 cycles, while C3TAg32 stabilised at ~0.40 after ~5500 cycles. C3TAu32 maintained the lowest and most stable COF (≈ 0.20 ± 0.05), confirming its superior tribological performance.

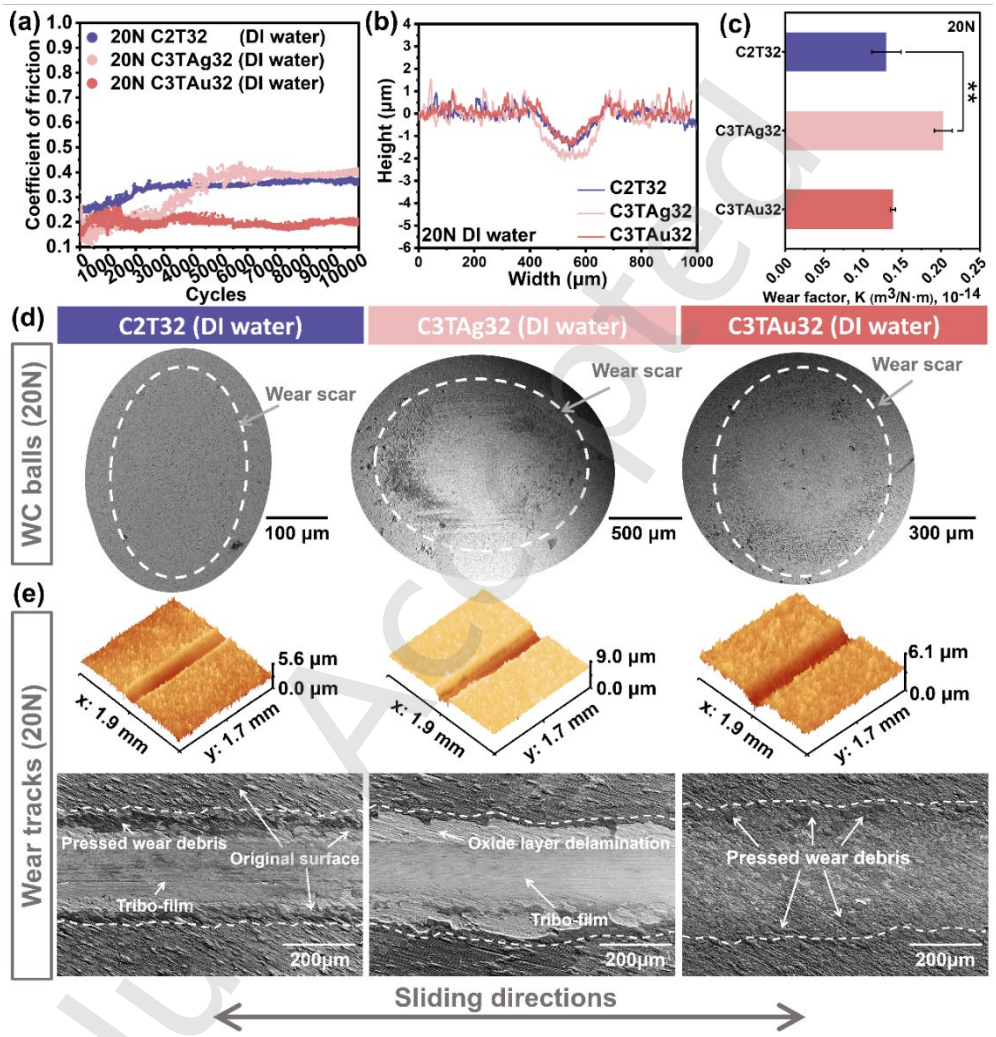

Figure 7. Tribological performance of the three IBTSF-treated Ti-15-3 surface systems in deionised water (DI water) during sliding under a load of 20 N. (a) COF; (b) 2D wear track profiles; (c) wear factors calculated from the wear track profiles; (d) SEM images of the corresponding wear scars on the WC counterpart balls; (e) 3D wear track morphologies and the corresponding SEM observations of the wear tracks. Error bars represent the standard deviation of three independent measurements (mean ± SD, n = 3). Statistical significance was analysed using one-way ANOVA (** $p < 0.01$).

The cross-sectional wear profiles (**Figure 7b**) show that the wear extent of these 3 surface systems follows the order: C3TAg32 > C3TAu32 > C2T32, with C3TAg32 and C2T32 exhibiting substantial reductions in wear depth compared with unlubricated condition. **Figure 7c** compares the wear factors of the 3 samples. For C3TAg32 and C2T32, the wear factors decreased dramatically from 2.7×10^{-13} and 2.73×10^{-13} $m^3/(N\cdot m)$ under unlubricated condition to 0.2×10^{-14} and 0.05×10^{-14} $m^3/(N\cdot m)$ in DI water, respectively. In contrast, the wear factor of C3TAu32 showed stable value relative to the unlubricated condition. **Figure 7d** displays the wear scars on the WC balls and the corresponding worn surfaces of the Ti-15-3 samples. On the counterpart surfaces, all 3 samples produced only fine scratches parallel to the sliding direction, without detectable Ti or O transfer. This indicates that abrasive wear dominated for all these samples in DI water. This transition from adhesive wear for unlubricated samples (**Figure 4**) to abrasive wear explains the reduced COF and the absence of the unstable, dispersed COF behaviour observed under unlubricated condition. Among these 3 samples, C2T32 showed the mildest wear on the WC ball, consistent with the presence of a continuous tribo-film on its wear track that effectively protected the surface. In contrast to its behaviour in oil, C3TAg32 formed a tribo-film in DI water, although partial delamination was observed. C3TAu32 exhibited the shallower wear scars than C3TAg32, likely due to the lubricating action of Au particles.

3.2.3 In simulated seawater

Further to the friction experiments conducted in DI water (**Section 3.2.2**), tribo-corrosion tests were further performed in SSW to evaluate the corrosion-wear behaviour of the three surface systems under corrosive-wear conditions. The results are summarised in **Figure 8**.

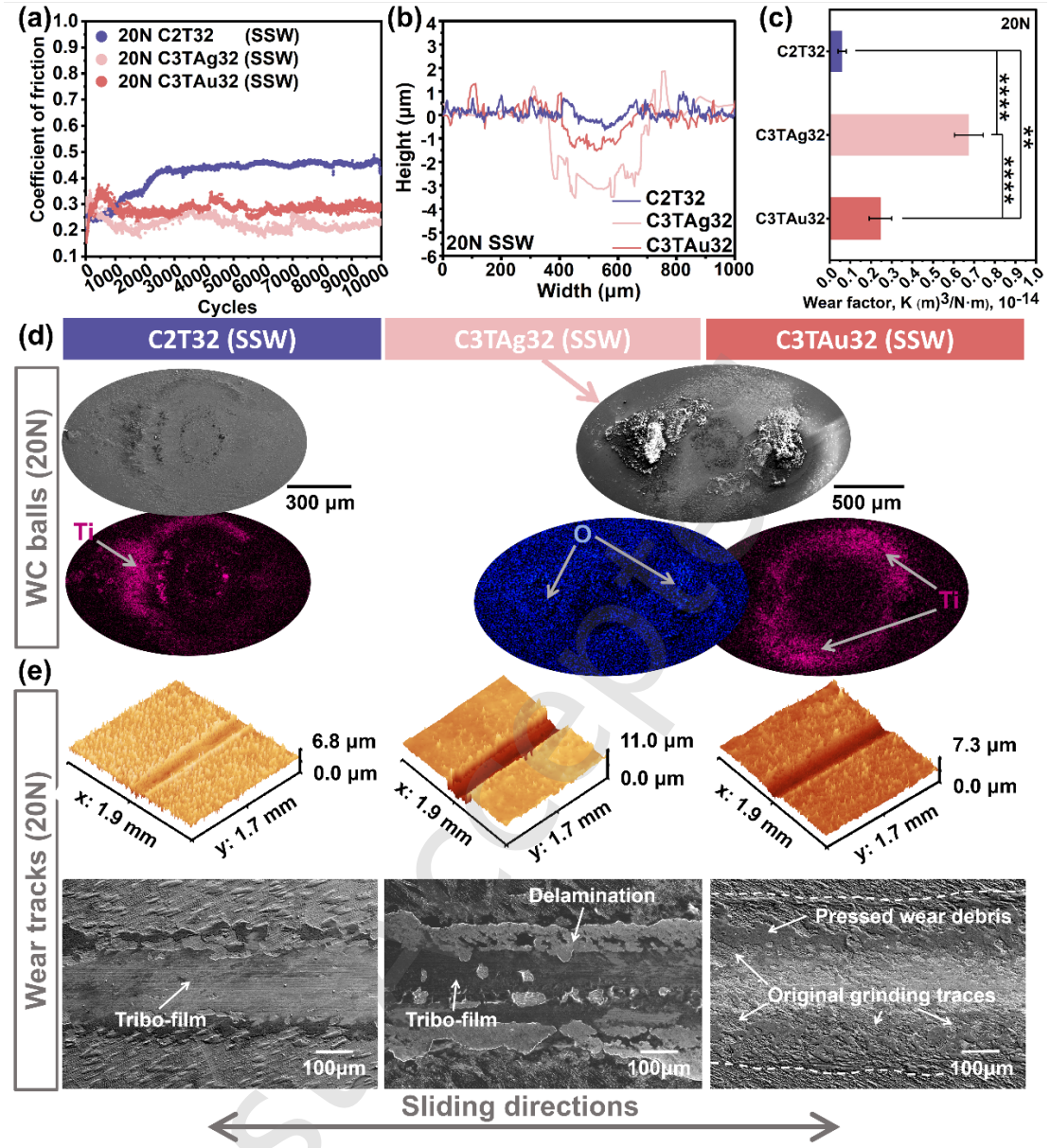

Figure 8. Tribological performance of the three IBTSF-treated Ti-15-3 surface systems in simulated seawater (SSW) during sliding under a load of 20 N. (a) COF; (b) 2D wear track profiles; (c) wear factors calculated from the wear track profiles; (d) SEM images of the corresponding wear scars on the WC balls, with Ti elemental (EDX) mapping for C2T32 and Ti/O elemental (EDX) mapping for C3TAg32; (e) 3D wear track morphologies and the corresponding SEM observations of the wear tracks. Error bars represent the standard deviation of three independent measurements (mean ± SD, n = 3). Statistical significance was analysed using one-way ANOVA (**p < 0.01, ****p < 0.0001).

As shown in **Figure 8a**, compared with the COF trends in DI water, the friction coefficients of C3TAu32 and C2T32 increased by approximately 0.05 in SSW, whereas that of C3TAg32 decreased markedly from ~0.40 to ~0.20. Despite its highest COF among the three samples (~0.45), the cross-sectional wear profiles in **Figure 8b** reveal that C2T32 exhibited the smallest wear area, while C3TAg32 showed the largest. Consequently, the wear rate of C2T32 remained the lowest, increasing only slightly from 0.05×10^{-14} $m^3/(N\cdot m)$ in DI water to ~0.06×10^{-14} $m^3/(N\cdot m)$ in SSW.

In contrast, the wear rate of C3TAg32 increased sharply from 0.20×10^{-14} in DI water to ~0.68×10^{-14} $m^3/(N\cdot m)$ in SSW, representing the largest deterioration among all the samples. C3TAu32 also exhibited a moderate increase in its wear rate, from 0.15×10^{-14} to 0.25×10^{-14} $m^3/(N\cdot m)$, when changing the DI water to SSW.

Overall, the comparison across the two aqueous environments indicates that C2T32 possesses the highest resistance to tribo-corrosion, whereas C3TAg32 is the most vulnerable in SSW. Additionally, C3TAg32 displayed two COF rises—one at the beginning of sliding and the other around 4000 cycles—likely corresponding to the repeated formation and failure of tribo-films, consistent with the mechanism discussed in **Figure 11**.

The observations of the wear scars of the WC balls and their EDX maps (**Figure 8d**) further support these findings. Transferred titanium was detected on all the counter-body surfaces. The counterpart WC balls sliding against C3TAg32 in SSW exhibited the most severe Ti transfer and adhesion, accompanied by substantial oxides accumulation on both sides of the sliding direction, which may partly explain its unstable COF in SSW. C3TAu32 and C2T32 showed comparatively mild Ti transfer, with minor abrasive marks.

The 3D wear topography provides a direct comparison of the wear severity. C3TAg32 suffered the most pronounced damage, and its SEM images revealed

a tribo-film within the wear track that was more heavily disrupted compared with the DI water environment. As inferred from **Figure 11**, this film originated from crushed oxide debris compacted under repeated loading, and the presence of chloride ions likely impaired film consolidation. C3TAu32 experienced moderate wear but showed deeper centre grooves than in DI water, indicating aggravated material removal in SSW. By contrast, C2T32 again showed the mildest wear, characterised mainly by shallow, sliding-direction scratches that match those observed on the WC ball—confirming that abrasive wear, rather than adhesive wear, remained dominant even under corrosive conditions.

4 Discussion

4.1 Wear performance comparison

Figure 9 summarises the wear factors of the three surface systems (C2T32, C3TAg32, C3TAu32) under five reciprocating sliding conditions: unlubricated under 10 N and 20 N, and under 20 N lubricated with oil, in DI water, and in SSW.

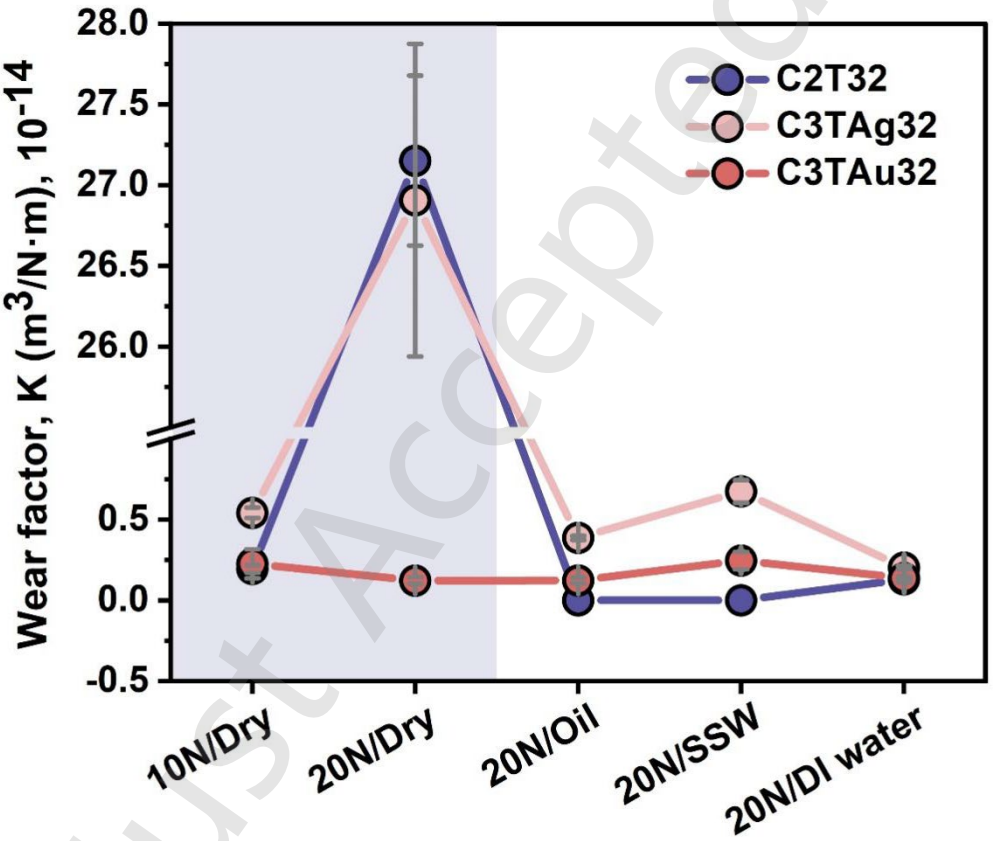

Figure 9. Comparison of the wear factors of C2T32, C3TAg32 and C3TAu32 under different tribological conditions (10 N unlubricated, 20 N unlubricated, 20 N oil, 20 N deionised water and 20 N simulated seawater).

Overall, C3TAu32 exhibited the most stable wear resistance across all conditions, maintaining a wear factor below ~0.25 × 10^{-14} $m^3/(N·m)$. Among all three samples, its performance is outstanding in unlubricated sliding, particularly at 20 N with its wear factor being at least two orders of magnitude lower than that for other two samples.

In contrast, C3TAg32 showed the overall poor wear performance, which may be related to the relatively poor integrity (multi-phased with coarse columnar TiO_2 and thick oxide layer (~3 μm) induced stress concentration and the resulting low interfacial adhesion of the surface oxide layer. In corrosive NaCl solution, its wear factor increased from 0.2×10^{-14} m³/(N·m) in DI water to more than triple (~0.7×10^{-14} m³/(N·m)), indicating its pronounced sensitivity to chloride-induced degradation.

Compared with both C3T samples, C2T32 demonstrated the best wear resistance under all three liquid environments, including oil, SSW, and DI water. In these liquid environments, its wear factors were even lower than that of C3TAu32. Under unlubricated conditions, although C2T32 performed well at a relatively low load of 10N, extremely high wear was recorded under 20 N. This is evidenced by the rapid increase of COF (**Figure 2b**) and typical adhesive wear features (**Figure 4b, c**), thus leading to the highest wear factor of ~2.72×10^{-13} m³/(N·m) (**Figure 9**).

In summary, the three surface systems exhibited environment-dependent wear behaviours: without lubrication, C3TAu32 performed best; C2T32 excelled under lubricated conditions but C3TAg32 offered an overall poor wear performance despite the attractive antibacterial function [10]. Motivated by these contrasting behaviours, the following sections are devoted to exploring the underlying mechanisms governing their different tribological responses to advance scientific understanding thus contributing to new knowledge.

4.2 Load effect in unlubricated contact

It is of interest to note from **Figure 9** that when tested under a low load of 10 N, all three treated samples showed a similar low wear factor although C3TAg showed a slightly higher wear factor than other two samples. However, when tested under a high load of 20 N, dramatically increased wear factors (more than 10 times) were observed for both C2T32 and C3TAg32, which could be

attributed to their surface layer structures and load-bearing capacities, the bonding strength, the doubled load and the relatively high coefficient of friction.

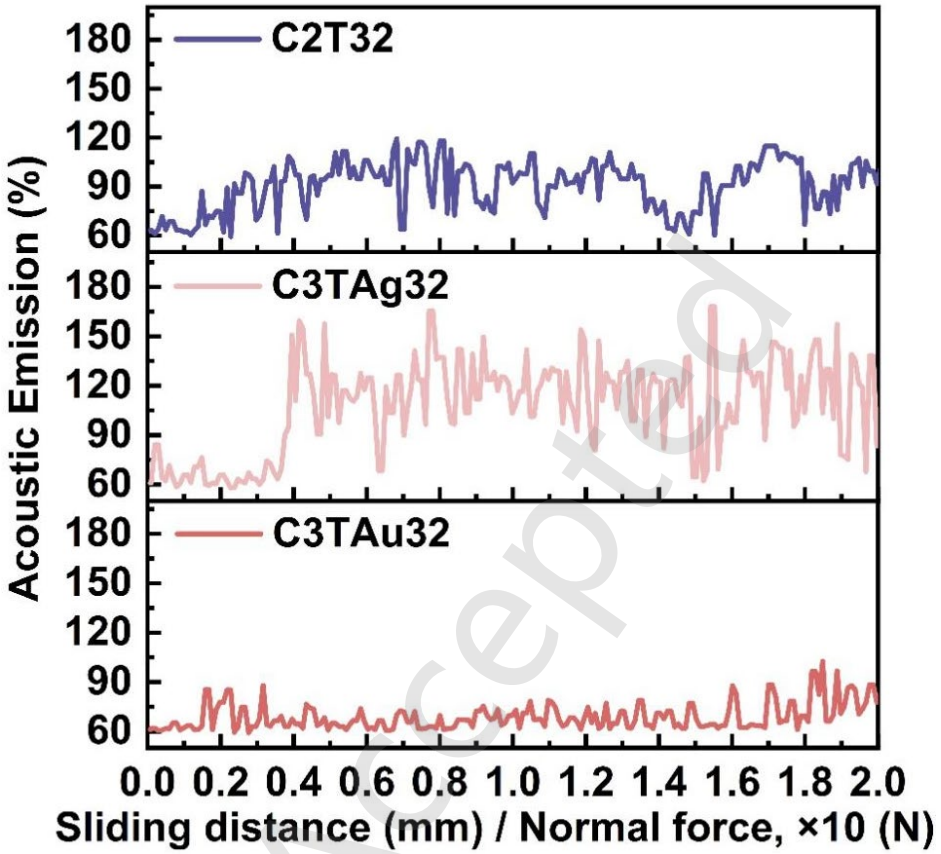

Figure 10. Acoustic emission (AE) responses recorded during progressive-load scratch tests of C2T32, C3TAg32 and C3TAu32.

To further evaluate the integrity of the oxide/substrate interface, scratch tests combined with acoustic emission (AE) monitoring were performed, as shown in **Figure 10**. The C3TAu32 sample exhibited consistently low AE signals throughout the entire loading process, indicating that no significant fracture or delamination of the oxide layer occurred during scratching. This behaviour suggests excellent mechanical integrity and strong oxide/substrate bonding. In contrast, C3TAg32 showed a sharp increase in AE intensity when the normal load reached approximately 4 N, implying the onset of local cracking or partial failure of the oxide layer. The C2T32 sample exhibited a similar transition at a much lower load of approximately 1.5 N, indicating the earliest initiation of surface damage among the three surface systems. These results demonstrate

that the interface stability follows the order C3TAu32 > C3TAg32 > C2T32, which is in good agreement with the tribological performance observed under unlubricated sliding conditions. The superior interface integrity of C3TAu32 effectively suppresses oxide layer fracture and delamination, thereby maintaining a stable tribological interface even under severe contact conditions. Although oxide thickness and surface hardness generally contribute to improving wear resistance, especially for C3TAg32, the tribological performance of the IBTSF-treated surfaces is governed by the combined effects of oxide thickness, oxide integrity and interface stability rather than by a single parameter. As summarised in **Figure 1**, the surface oxide formed on C2T32 is very thin (~0.8 μm) and hence its load bearing capacity is expected to be very low. Therefore, the thin surface oxide layer on soft Ti substrate was damaged quickly under the high normal pressure from the applied load. This is caused by the so-called 'egg shell effect' [23], which occurs when a hard and thin layer on a soft substrate is loaded under a high stress. This is supported by the rapid increase of COF after about 100 cycles, indication of the damage and removal of the surface oxide layer. This is followed by a very high & fluctuating COF (**Figure 2b**), which is typical stick-slip friction behaviour of untreated Ti and its alloys [7]. Accordingly, very high wear factor was recorded and severe adhesive wear features were observed on the wear track (**Figure 4b**).

Although the oxide layer formed on C3TAg32 is much thicker (~3.0 μm) than that formed on C2T32, large wear factor close to that for C2T32 (**Figure 9**) and very high COF (**Figure 2b**) was also observed when tested under the high load of 20 N in unlubricated contact. As described in **Section 3.1.1**, the wear of C3TAg32 can be divided into 3 stages. Wear of the oxide layers occurred mainly due to its large columnar grains [10], and the wear debris was compacted to form a tribo-film within Stages I & II (**Figure 11**). Hence, the wear factors are relatively small and the COF increased gradually. However, when the tribo-film was worn away by repeated reciprocation sliding and the COF started to

increase further in Stage III. Eventually, the residual oxide layer was removed because of the increased tangential shear force during sliding and stress concentration at the oxide/substrate interface due to the formation of very thick oxide layer, which led to the weak interface bonding [24, 25]. Accordingly, this led to direct contact between WC ball and Ti substrate and severe adhesive wear, which is confirmed by the typical adhesive wear features on the wear track and the transferred Ti to the WC counterpart (**Figure 4b, c**).

In contrast, the wear factor for C3TAu32 remained unchanged or even marginally reduced, and the COF increased slowly with the increase of the reciprocating cycles when the applied load was doubled. This desirable tribological behaviour can be attributed to the very dense oxide layer with an optimal thickness of about 1.6 μm, and the unique distribution of catalytic elements within the surface layer, leading to different oxide/substrate interaction with C3TAg32. According to our recent study [10], Au is mainly on the oxide surface and enriched near the oxide/substrate interface of the C3TAu32. It has been reported that, as a soft solid lubricant, Au particles et al. can effectively reduce friction [26-29]. Thus, the surface Au particles contribute to friction reduction through a self-lubricating effect. While the interfacial Au expended the actual contact area, thereby improving the bonding strength and the stability of the oxide/substrate interface. Additionally, the optimised oxide layer thickness can, on one hand, avoid the ‘eggshell effect’ of very thin oxide layer on soft substrate as observed for the C2T32 sample; on the other hand, it can prevent interface stress concentration induced spallation of oxide layer as observed for the C3TAg32 sample. In contrast, Ag is mainly distributed throughout the oxide layer and primarily promotes oxide growth, resulting in a thicker oxide layer but providing less improvement in surface wear resistance and interface stability. It is the combination of the low friction (hence the low tangential shear force), satisfactory interface bonding and adequate load bearing capacity that confers the outstanding tribological performance of C3TAu32 even under the high

applied load of 20 N.

From an industrial perspective, it should be noted that the Au deposited in the present study functions solely as an ultrathin catalytic film to modify the oxidation kinetics during the IBTSF process, rather than as a conventional functional coating. Hence, the amount of Au required is extremely small due to its nanoscale thickness (~20 nm), corresponding to only approximately ~0.39 g/m^2 of Au (equivalent to ~£37 /m^2 based on a representative market price of ~£97 /g), resulting in only a marginal increase in processing cost. Moreover, the superior tribological performance is primarily provided by the dense ceramic conversion layer formed during treatment rather than by the Au itself. Therefore, the additional cost associated with the catalytic Au layer can be justified in high-value engineering applications, such as aerospace and biomedical components.

4.3 Fluid effect under 20 N

As depicted in **Figure 9**, when tested under 20 N, while C3TAu32 showed almost constant or marginally increased wear factors in liquid environments, the wear factors for both C2T32 and C3TAg32 dramatically reduced mainly by the lubrication effect of the liquids including oil, SSW and DI water. Likewise, the COFs are effectively reduced from about 0.40-0.72 in unlubricated contact (**Figure 2b**) to 0.10-0.15 in oil (**Figure 6a**), 0.20-0.35 (**Figure 7a**) in DI water, and 0.30-0.50 in SSW (**Figure 8a**).

It is of great interest to notice that although C2T32 showed the highest wear factor under unlubricated condition mainly due to the low load bearing capacity, it revealed the lowest wear factor among all the three types of samples in all three fluids. This is because fluids, both lubricating fluids (e.g. oil) and non-lubrication fluids (e.g. DI water), can redistribute load and reduce contact stress [30]. Therefore, the C2T32 sample can withstand the reduced contact stress due to the fluids used thus avoiding the severe surface damage as observed in unlubricated contact.

It is also observed from **Figure 9** that the wear factor of C2T32 gently increased in the order of in oil, SSW and DI water and that the start COFs increased from about 0.10 in oil to about 0.25 in SSW and DI water. The examinations of the wear tracks formed provided evidence of boundary lubrication when tested in all three fluids. As shown in **Figure 6**, **Figure 7** and **Figure 8**, direct contact between the counterpart WC ball and the sample surfaces occurred during the tests in the fluids used as evidenced by the 2D wear track depth profiles and the 3D surface morphologies. Even for oil lubricated sliding test, wear tracks can be clearly identified from the 2D wear track depth profile (**Figure 6b**) wear track morphologies (**Figure 6d**). This is understandable from lubrication theory in view of the very low sliding speed of 5 mm/s and relatively high surface roughness values (**Figure 1**).

The effect of the three fluids on the wear factors C2T32 under boundary lubrication conditions are believed to be related to their viscosities. According to lubrication theory, when tested under the same contact conditions (load, speed), the thickness of the lubrication films (h) is decided mainly by the viscosity of the lubricants. Therefore, for the given surfaces of the ball and the plate, and hence the resulting combined root mean square of the surface roughness (σ), the Lambda ratio $\lambda = h/\sigma$, the measure of effectiveness of the boundary lubrication, is closely related to the viscosity of the lubricants. The dynamic viscosity of the oil used in this study at about 20 °C is much larger (>100 mPa·s) than that for SSW (1.05 mPa·s) and DI water (1.00 mPa·s). Hence, low COF (~0.10) and no measurable wear are expected for C2T32 in oil lubricated condition. Although both C3T samples are characterised by low friction, the wear factors for these two samples are higher, being about 0.12 × 10^{-14} $m^3/(N·m)$ and 0.39 × 10^{-14} $m^3/(N·m)$ for C3TAu32 and C3TAg32 respectively (**Figure 6c**). This is because the surface roughness (Ra) of C3TAu32 (0.28 μm) and C3TAg32 (0.43 μm) is higher than that for C2T32 (0.18 μm) and the lambda ratio and hence the effectiveness of lubrication of the C3T

samples is lower than the C2T sample. This is supported by the wear factors (**Figure 6c**) and the wear track morphologies observed (**Figure 6d**).

It is seemingly contradicting to note that the wear factor of C3TAg32 is larger when tested in oil (0.39×10^{-14} $m^3/(N \cdot m)$) than in DI water (0.22×10^{-14} $m^3/(N \cdot m)$). Close observation of the depth profiles of the wear tracks formed under these two conditions uncovered that although the maximum depth of the wear tracks is similar (about 1.9-2.0 μm), the shapes and the widths of these two wear tracks differ a lot. The wear track formed in oil lubrication is rectangle-shaped with a width about 350 μm (**Figure 6b**) whilst that formed in DI water is bell-shaped with a maximum width about 250 μm at surface. This implies that part of the oxide layer formed on C3TAu32 might have spalled during the tribo-action in oil whilst gradual wear by the WC ball occurred in DI water. The observation of the surface of the wear tracks disclosed that the wear track formed in oil lubrication (bottom-middle image in **Figure 6d**) differs greatly from the as-treated surfaces along the clearly defined parallel edges of the wear track; on the other hand, the wear track formed in DI water (bottom-middle image in **Figure 7d**) was covered with some tribo-films with zig-zag edges. The higher wear rate of C3TAg32 when tested with oil lubrication than tested in DI water could be related to the local high oil pressure and the multi-layered course columnar oxide structure as schematically shown in **Figure 11a**.When tested in DI water, due to the low viscosity and sloe sliding speed, no lubrication film could be formed and the load is directly supported by asperity-to-asperity contact. However, when tested in oil at low sliding speed, isolated oil films would form at some local areas although they cannot fully separate solid surfaces (i.e. boundary lubrication). The applied load is partially supported by asperity-to-asperity contact and partially supported by the lubricating oil films. Under the high pressure, oil could penetrate through the columnar gaps to reach the oxide layer and the substrate interface. As has discussed above, large stress concentration at the exists oxide/substrate due to the differences in physical

and mechanical properties between the surface oxide layers (ceramic) and the Ti substrate (metallic) especially for the thick (3.0 μm) oxide layer formed on C3TAg32. Accordingly, interface debonding resulted the spallation of the surface oxide layer under the joint action of concentrated stresses and oil pressure.

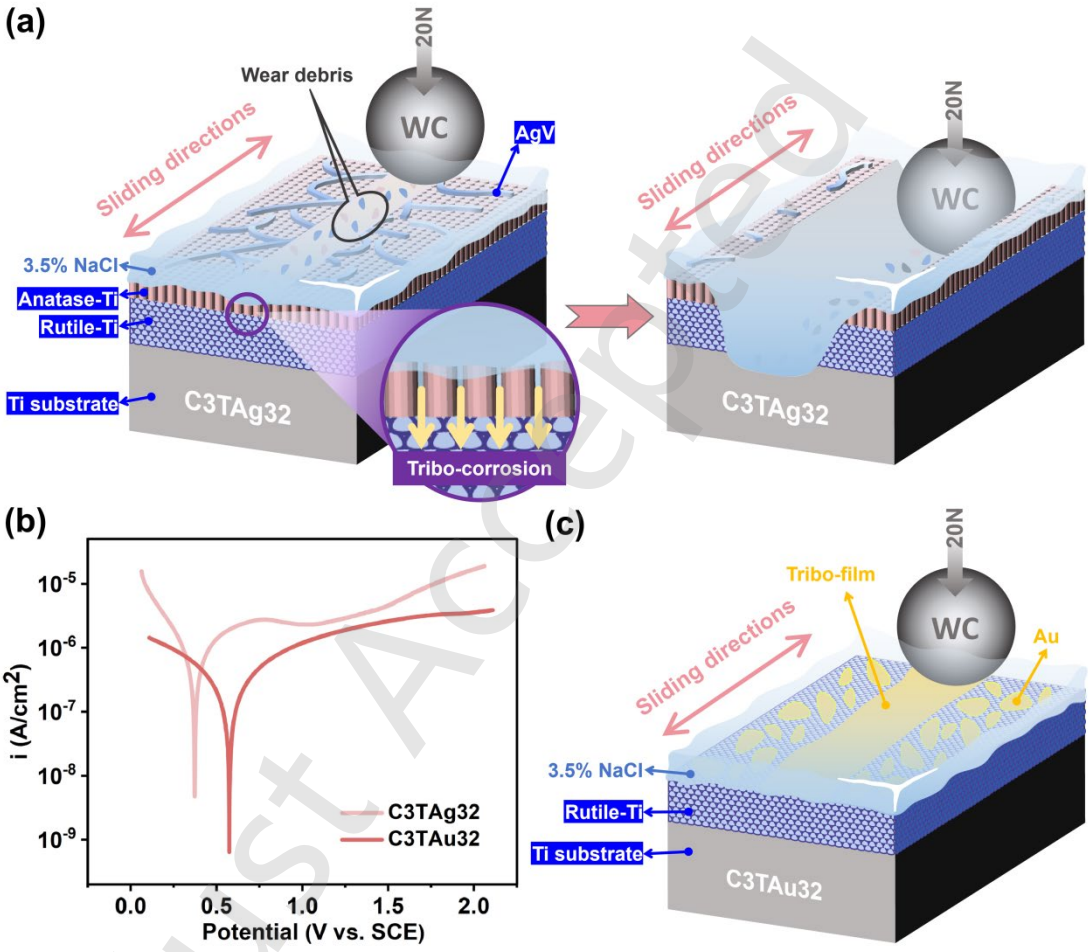

Figure 11. Proposed wear mechanisms of the IBTSF-treated Ti-15-3 surface systems in simulated seawater (SSW): (a) schematics of the wear mechanism of C3TAg32; (b) polarisation curves of C3TAg32 and C3TAu32 measured in SSW; (c) schematic of the wear mechanism of C3TAu32.

The highest wear factor of 0.65 × 10^{-14} $m^3/(N \cdot m)$ (**Figure 9**) among the three types of samples tested in three fluids was observed for C3TAg32 when tested in SSW, and the possible causes are considered to be twofold (**Figure 9a**). Firstly, as schematically shown in **Figure 11b**, the corrosion performance of

C3TAg32 in SSW containing 3.5% NaCl is poor as evidenced by the low corrosion potential and high corrosion current density, and corrosion would occur during the tribo-test (i.e. tribo-corrosion). During sliding, Ag/AgV exposed at or near the oxide surface is susceptible to electrochemical reactions with Cl^- containing electrolyte. The interaction between Ag^+ and Cl^- ions locally destabilises the tribo-film and facilitates its removal under repeated sliding [31]. Hence, fresh material is continuously exposed to the corrosive environment, accelerating the synergistic effect of corrosion and mechanical wear. This tribo-corrosion process results in the significantly increased wear factor observed for C3TAg32 in SSW. Secondly, as has been reported [10] and summarised in **Figure 1**, the oxide case formed on C3TAg32 is multi-layered: a thin and hard AgV oxide film atop a coarse columnar structured anatase TiO_2 layer, which is followed by a rutile TiO_2 layer on the substrate. Therefore, when the superficial hard AgV oxide film was removed by the corrosion-wear, the vertical intercolumnar interfaces were exposed to the solution. Under the liquid pressure, the corrosive solution was forced to penetrate the oxide layer through the intercolumnar gaps, thus leading to the spallation of the anatase TiO_2 layer (**Figure 11a**). With the continuation of the tribo-corrosion test, the wear debris specially form the very hard AgV oxide would act as abrasives to cause even more severe corrosion-wear to the rutile oxide layer. Eventually, the whole oxide case was removed as is evidenced by the fact that the wear track is deeper (3.5~4.0 μm) than the whole oxide thickness (3.0 μm) and that lumps of transferred Ti was found on the WC ball surface (**Figure 8**). In addition, the slightly high wear fact for C3TAu32 in SSW than in DI water suggested corrosion-wear effect but it is very limited partially because of its good corrosion behaviour and partially because of dense rutile oxide layer (**Figure 11c**).

Consequently, the roles of Au and Ag in determining the tribological behaviour are strongly dependent on the lubrication environment. During unlubricated sliding, where actual contact area, the self-lubricating effect of the surface Au

particles effectively reduces the frictional shear stress, enabling C3TAu32 to exhibit the lowest coefficient of friction and wear. In contrast, Ag mainly promotes oxide growth, resulting in a thicker oxide layer with characteristic AgV surface features, but provides a less friction-reducing effect than Au due to its high surface hardness value (~1200 HV) [10]. Under liquid conditions, however, the interaction between the liquid phase and the surface oxide layer gradually becomes the dominant factor governing tribological behaviour. Under oil lubrication condition, a continuous lubricant film effectively separates the sliding interfaces, largely replacing the self-lubricating function of the catalytic elements. Thus, the coefficients of friction of all three surface systems become super low (~0.1) and not comparable. In DI water, the low viscosity of water allows actual contact area interaction to remain significant. Meanwhile, water molecules readily adsorb onto the TiO_2 surface to form hydroxylated interfaces [32], facilitating cooling and wear debris removal. As a result, the self-lubricating effect of Au remains effective, enabling C3TAu32 to maintain the lowest coefficient of friction. Under SSW conditions, Cl^- ions introduce tribo-corrosion by destabilising the oxide layer and accelerating its degradation under reciprocating sliding wear. Hence, the Ag-containing surface becomes more susceptible to Cl^--induced degradation, leading to inferior wear resistance. Nevertheless, the reaction products generated during sliding are considered to reduce the frictional shear stress, accounting for the relatively low coefficient of friction of C3TAg32 despite its accelerated wear. Overall, these results demonstrate that while the catalytic particles dominate the tribological behaviour under unlubricated friction, the structural stability of the oxide layer and its interaction with the surrounding liquid become the controlling factors under liquid conditions.

5 Conclusions

The tribological behaviour of IBTSF-treated Ti-15-3 β-titanium alloy was investigated under reciprocating sliding conditions in three fluids, including lubricating fluid of oil and non-lubrication fluids of DI water and SSW, for up to 10,000 cycles. The results show that the friction and wear responses are strongly dependent on the load and lubrication environments.

- Under unlubricated conditions, although the conventional ceramic conversion treated (C2T32) Ti-15-3 β-titanium alloy reveal a low wear factor when tested under a low load of 10 N, severe wear occurred under a high load of 20 N due to its low load bearing capacity.
- The novel IBTSF-treated C3TAu32 exhibited the most stable friction behaviour and the lowest wear factor, even at a high normal load of 20 N without lubrication, owing to its good oxide layer integrity, high interfacial bonding strength, and the lubricating effect of Au.
- When tested in oil and SSW, the conventional ceramic conversion treated C2T32 showed superior wear property to the IBTSF-treated C3TAg32 and C3TAu32 although the frictional behaviour of C2T32 is inferior to C3TAg32 and C3TAu32 in SSW.
- The wear factor of C3TAg32 is much higher when tested in SSW than in DI water clearly indicating the corrosion wear nature of C3TAg32 in the presence of chloride ions.

Overall, the tribological behaviours of the IBTSF-treated C3TAg32 and C3TAu32 in particular are superior to the conventionally treated C2T32 mainly due to the self-lubricating effect of Ag and Au and their relatively higher load bearing capacity; however, C2T32 outperformed C3TAg32 and C3TAu32 when tested in fluids. Therefore, the IBTSF-treated C3TAu32 is recommended for unlubricated applications while C2T32 is the best for marine or oil lubricated applications.

Acknowledgement

The authors gratefully acknowledge **XXX** for providing access to the white light interferometer. **XX** acknowledges support from the National Natural Science Foundation of China (52501024) and from the Young Talent Support Project of Guangzhou Association for Science and Technology (No. QT-2025-041).

References

[1] P. Han, L. Ni, W. Wang, K. Zhou, H. Yang, J. Lin, K. Qiao, F. Qiang, J. Cai, Q. Wang, Superplastic deformation behaviors of fine-grained Ti-15 V-3Cr-3Al-3Sn alloy prepared via ultra-low heat input friction stir processing, Materials Characterization 215 (2024) 114229.

[2] W. Zhang, K. Wang, X. Qi, H. Liu, A. Li, H. Ding, H. Fujii, W. Liu, Superplastic behavior of a metastable β-type Ti alloy governed by grain size: Microstructure evolution and underlying deformation mechanism, Materials Science and Engineering: A 915 (2024) 147212.

[3] H. Lu, P. Ji, B. Li, W. Ma, B. Chen, X. Zhang, X. Zhang, M. Ma, R. Liu, Mechanical properties and deformation mechanism of a novel metastable β-type Ti–4V–2Mo–2Fe alloy, Materials Science and Engineering: A 848 (2022) 143376.

[4] J.L. Neves, T. Wojcik, D. Obersteiner, J. Grillitsch, D. Holec, D. Kiener, T. Klein, Wire-Arc directed energy deposition of metastable-β alloy Ti-15 V-3Cr-3Sn-3Al using thick wire feedstock: Microstructure and mechanical response, Materials & Design (2025) 114757.

[5] T.-M. Chiu, M. Mahmoudi, W. Dai, A. Elwany, H. Liang, H. Castaneda, Corrosion assessment of Ti-6Al-4V fabricated using laser powder-bed fusion additive manufacturing, Electrochimica Acta 279 (2018) 143-151.

[6] X. Xu, W. Li, B. Wan, S. Jin, K. Chen, F. Su, Extremely improved the corrosion resistance and anti-wear behavior of aluminum alloy in 3.5% NaCl solution via amorphous CrAlN coating protection, Corrosion Science 230 (2024) 111952.

[7] L. Hu, Z. Wang, J. Wang, Y. Wang, Derivative analysis and evaluation of roll-slip fretting wear mechanism of ultra-thin-walled bearings under high service, Wear 562 (2025) 205630.

[8] P. Perera, K. Hayward, F. Guzzomi, A. Vafadar, Erosion wear characterisation of an open Ductile Iron butterfly valve subjected to Aluminium

Oxide particle slurry flow, Tribology International 191 (2024) 109199.
[9] K. Hua, Y. Tong, F. Zhang, C. Wang, H. Kou, H. Wu, H. Wang, Dependence of fretting wear on the microstructure characteristics and impact on the subsurface stability of a metastable β titanium alloy, Tribology International 165 (2022) 107351.
[10] T. Pan, X. Huang, B. Dashtbozorg, S. Sun, Y. Yang, K. Ren, A. Stamboulis, X. Li, K. Ma, H. Dong, Novel surface engineering design enabled surface multi-functionalisation of metastable Ti-15-3 β-titanium alloy, Friction (2026).
[11] P. Miller, J. Holladay, Friction and wear properties of titanium, Wear 2(2) (1958) 133-140.
[12] K. Zheng, X. Zhao, L. Pan, Z. Ren, Ultrasonic rolling strengthening of TC11 titanium alloy surface: Corrosion and wear properties under extreme conditions, Wear 550 (2024) 205415.
[13] X. Guo, M. Ma, S. Zhang, Z. Wei, Microstructure and wear resistance of tungsten carbide particle reinforced titanium alloy coating by WAAM, Tribology International 194 (2024) 109536.
[14] X. Li, H. Dong, Ceramic conversion treatment of titanium-based materials, Surface Engineering of Light Alloys, Elsevier2010, pp. 475-500.
[15] C. Li, D. Horspool, H. Dong, Effect of ceramic conversion surface treatment on fatigue properties of Ti6Al4V alloy, International journal of fatigue 29(12) (2007) 2273-2280.
[16] E. Redmore, X. Li, H. Dong, Tribological performance of surface engineered low-cost beta titanium alloy, Wear 426 (2019) 952-960.
[17] Y. Yang, C. Zhang, Y. Dai, J. Luo, Tribological properties of titanium alloys under lubrication of SEE oil and aqueous solutions, Tribology International 109 (2017) 40-47.
[18] H. Hong, A. Riga, J. Gahoon, C. Scott, Machinability of steels and titanium alloys under lubrication, Wear 162 (1993) 34-39.
[19] F. Mansfeld, G. Liu, H. Xiao, C. Tsai, B. Little, The corrosion behavior of

copper alloys, stainless steels and titanium in seawater, Corrosion science 36(12) (1994) 2063-2095.
[20] Y. Sun, R. Bailey, J. Zhang, Y. Lian, X. Ji, Improving oil lubrication effectiveness of Ti-Ti tribopair by thermal oxidation, Surface and Coatings Technology 512 (2025) 132346.
[21] T. Pan, X. Li, Z. Zhang, Y. Yang, C. Liu, G. Qiao, H. Huang, H. Dong, A novel surface engineering technique for improving tribological performance of low-cost beta titanium alloy, Wear 572 (2025) 206076.
[22] I. Hutchings, P. Shipway, Tribology: friction and wear of engineering materials, Butterworth-heinemann2017.
[23] H. Dong, T. Bell, Tribological behaviour of alumina sliding against Ti6Al4V in unlubricated contact, Wear 225 (1999) 874-884.
[24] Q. Zhou, L. Yang, C. Luo, F. Chen, Y. Zhou, Y. Wei, Thermal barrier coatings failure mechanism during the interfacial oxidation process under the interaction between interface by cohesive zone model and brittle fracture by phase-field, International Journal of Solids and Structures 214 (2021) 18-34.
[25] W. Li, Z. Yang, P. Wang, L. Liu, Y. Wang, S. Wang, L. Chang, L. Ma, Effect of different oxidation modes on the growth of oxide layer of TC11 titanium alloy, Journal of Materials Research and Technology 32 (2024) 4265-4277.
[26] M. Antler, The lubrication of gold, Wear 6(1) (1963) 44-65.
[27] M.H. Kabir, D. Dias, M. Velhal, H. Liang, Effects of oxidation-assisted grafting of MoS2 on tribological performance of steels, Tribology International 211 (2025) 110826.
[28] Z. Chen, C. Gao, X. Pei, M. Hu, Y. Du, T. Yang, B. Bou-Saïd, H. Wang, Recent advances and optimization strategies in tribological performance of high entropy alloys, Tribology International (2026) 112089.
[29] W. Ye, Y. Shi, Q. Zhou, M. Xie, H. Wang, B. Bou-Saïd, W. Liu, Recent advances in self-lubricating metal matrix nanocomposites reinforced by carbonous materials: A review, Nano Materials Science 6(6) (2024) 701-713.

[30] T. Fischer, M. Luton, Influence of Lubricating and Nonlubricating Fluids on the Stress Distribution and Surface Deformation in Sliding Contacts in the Absence of Hydrodynamic Effects, Tribology Series, Elsevier1981, pp. 683-695.
[31] J. Tabor, C.-Y. Li, The effect of an aqueous environment on the surface hardening of silver chloride, Acta Metallurgica 15(12) (1967) 1861-1865.
[32] P. Dong, Y. Zhang, S. Zhu, Z. Nie, H. Ma, Q. Liu, J. Li, First-principles study on the adsorption characteristics of corrosive species on passive film TiO2 in a NaCl solution containing H2S and CO2, Metals 12(7) (2022) 1160.